

Phase diagram of the Gaussian-core model

Santi Prestipino,^{1,*} Franz Saija,^{2,†} and Paolo V. Giaquinta^{1,‡}

¹*Dipartimento di Fisica, Università degli Studi di Messina, Contrada Papardo, 98166 Messina, Italy*

²*Istituto per i Processi Chimico-Fisici del CNR, Sezione di Messina, Via La Farina 237, 98123 Messina, Italy*

(Received 19 February 2005; revised manuscript received 12 April 2005; published 26 May 2005)

We trace with high numerical accuracy the phase diagram of the Gaussian-core model, a classical system of point particles interacting via a Gaussian-shaped, purely repulsive potential. This model, which provides a reliable qualitative description of the thermal behavior of interpenetrable globular polymers, is known to exhibit a polymorphic fcc-bcc transition at low densities and reentrant melting at high densities. Extensive Monte Carlo simulations, carried out in conjunction with accurate calculations of the solid free energies, lead to a thermodynamic scenario that is partially modified with respect to previous knowledge. In particular, we find that: (i) the fluid-bcc-fcc triple-point temperature is about one third of the maximum freezing temperature; (ii) upon isothermal compression, the model exhibits a fluid-bcc-fcc-bcc-fluid sequence of phases in a narrow range of temperatures just above the triple point. We discuss these results in relation to the behavior of star-polymer solutions and of other softly repulsive systems.

DOI: 10.1103/PhysRevE.71.050102

PACS number(s): 64.10.+h, 05.20.Jj, 61.20.Ja, 64.70.Kb

It is common knowledge that crystallization is induced by the strong Pauli repulsion between inner-shell electrons, causing the *effective* interatomic potential to blow up at short distances. However, the existence of a thermodynamically stable solid phase does not necessarily require a singular repulsion for vanishing interatomic separations. As a matter of fact, a finite square barrier, equal to a positive constant ϵ for distances smaller than a given diameter σ being zero otherwise, is an example of a bounded repulsion that supports a stable solid at all temperatures [1,2]. In this respect, a Gaussian-shaped potential

$$v(r) = \epsilon \exp(-r^2/\sigma^2), \quad (1)$$

is a more realistic finite-strength repulsion. The so-called Gaussian-core model (GCM) was introduced by Stillinger [3]. Such a potential, despite the fact that it is finite even at full overlap between the particles, is nonetheless perfectly admissible as an effective potential. Actually, it is used to represent the entropic repulsion between (the centers of mass of) self-avoiding polymer coils dispersed in a good solvent [4–6]. Two distinctive features of the GCM, which are absent in the simpler penetrable-sphere system, are: (i) the existence of a maximum freezing temperature, T_{\max} and (ii) the occurrence, below T_{\max} , of reentrant melting into a dense fluid phase. Stillinger noted in his original paper that, in the limit of vanishing temperature and density, the GCM particles practically behave as hard spheres with increasingly large diameter. In this limit, the fluid freezes into a face-centered-cubic (fcc) structure at a temperature $T_f(\rho)$ that vanishes with the number density ρ (from now on, temperature and density will be given in reduced units, $T^* = k_B T / \epsilon$, where

k_B is Boltzmann's constant, and $\rho^* = \rho \sigma^3$). Indeed, a straightforward calculation of the total energy of different cubic crystal structures shows that the fcc structure is favored, at zero temperature, only for reduced densities lower than $\pi^{-3/2} \approx 0.1796$. Beyond this threshold, a body-centered-cubic (bcc) solid takes over. However, upon compression, any regular arrangement of particles is eventually destined to collapse for any $T > 0$ (reentrant melting) [7].

A comprehensive study of the phase diagram of the GCM was recently carried out by Lang and co-workers [4]. These authors employed an approximate integral-equation theory to describe the disordered phase and a variationally adjusted harmonic interaction for the crystalline phases. The resulting phase diagram (see Fig. 9 of Ref. [4]) accounts for the existence of a fluid phase and two solid phases. More specifically, the solid was found to be thermodynamically stable for temperatures lower than $T_{\max}^* = 0.0102$, a temperature at which the freezing line attains its maximum value for $\rho_{\max}^* = 0.2292$. The phase diagram displays a fluid-bcc-fcc triple point that was estimated to fall at $T_{tr}^* = 0.00875$. The fcc phase turns out to be stable below T_{tr}^* in the low-density region (for ρ^* less than ≈ 0.17), whereas the bcc structure prevails for larger temperatures and densities.

A parallel numerical study of the phase diagram of star-polymer solutions in a good solvent was carried out under a different assumption for the effective pair potential, modeled with an ultrasoft logarithmic repulsion within a diameter σ and with a Yukawa potential outside the core [8]. In this case, Monte Carlo (MC) simulations and free-energy calculations lead to a phase diagram that shows a rather complicated interplay between various cubic phases. It is desirable to have a similarly full-fledged analysis also for the GCM.

To this purpose, we performed standard Metropolis MC simulations of the GCM, keeping the number of particles N , the volume V , and the temperature T constant. We used the particle-insertion method [9] and the Frenkel-Ladd technique [10,11] to calculate the “exact” free energies of the dilute fluid and of the solid phases, respectively. By this means, we discovered that the phase diagram of the GCM is highly

*Corresponding author. Electronic address:

Santi.Prestipino@unime.it

†Electronic address: saija@me.cnr.it

‡Electronic address: Paolo.Giaquinta@unime.it

TABLE I. Excess Helmholtz free energy per particle f_{ex} , in units of $k_B T$, calculated for some fcc ($N=1372$) and bcc ($N=1458$) solid states of the GCM. For $T^*=0.003$ and 0.006 , the tabulated values refer to systems with 864 and 1024 particles, respectively. For each state and solid structure, we also display (within square brackets) the value of the reduced elastic constant $c^*=c\sigma^2/\epsilon$ that intervenes in the Frenkel-Ladd calculation: for the given c , the mean square displacement of the Einstein crystal approximately matches the mean square deviation of a GCM particle from its reference crystal site. For a number of selected ρ^* and T^* , we verified that the quantity $\beta f_{\text{ex}}(N) + \ln N/N$, with $\beta=(k_B T)^{-1}$, scales linearly with N^{-1} for large N , in agreement with a conjecture formulated in [11].

ρ^*	T^*	$\beta f_{\text{ex}}^{\text{(FCC)}}$	$\beta f_{\text{ex}}^{\text{(BCC)}}$
0.30	0.0020	195.703(2) [0.30]	195.312(1) [0.45]
0.24	0.0030	86.251(2) [0.35]	86.057(1) [0.39]
0.24	0.0033	78.994(1) [0.34]	78.814(1) [0.38]
0.24	0.0035	74.835(1) [0.33]	74.666(1) [0.38]
0.24	0.0037	71.122(2) [0.33]	70.961(1) [0.38]
0.24	0.0038	69.411(2) [0.32]	69.254(1) [0.37]
0.30	0.0040	101.074(2) [0.29]	100.894(1) [0.42]
0.24	0.0060	46.025(2) [0.29]	45.929(1) [0.35]
0.24	0.0080	35.781(2) [0.24]	35.710(1) [0.31]

elaborate [4], showing elements of similarity with the phase diagram of star-polymer solutions.

Our samples typically consisted of 1372 particles for the fluid and the fcc solid, and of 1458 particles for the bcc solid. Occasionally, we considered smaller as well as larger sizes, so as to check whether our conclusions were possibly undermined by a significant finite-size dependence. We paid much care to a safe estimate of statistical errors. This is actually an important issue whenever different crystalline structures so closely compete, as in the present case, for thermodynamic stability. We computed the free-energy difference between any two equilibrium states of the system belonging to the same phase through standard thermodynamic integration. This method allows one to obtain the properties of the model for any state, provided that the absolute free energy has been autonomously computed in at least one reference state per phase. Table I gives the excess Helmholtz free energy for some fcc and bcc states of the model. Though we did not systematically check the relative stability of other crystalline structures, we verified that, for temperatures close to the triple point, the hexagonal-close-packed (HCP) solid is slightly less favored than the fcc solid, while the simple-cubic solid is not mechanically stable.

The thermodynamically stable phase, for a given temperature and pressure, is the one with the lowest chemical potential $\mu(T, P)$. Figure 1 shows the difference between the chemical potentials of competing phases plotted as a function of P at fixed temperature. The sequence of phase transitions undergone by the GCM at $T^*=0.002$, with increasing pressures, is fluid-fcc-bcc-fluid: the disordered phase is actually seen to reenter the phase diagram at high density. As is also apparent from Fig. 1, the μ gap between the fcc and bcc phases is anything but monotonous when plotted as a func-

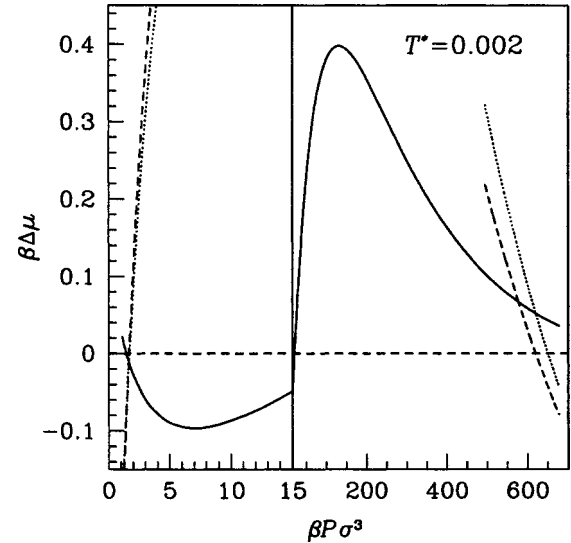


FIG. 1. Difference between the chemical potentials of pairs of GCM phases plotted as a function of the pressure along the isotherm $T^*=0.002$: $\beta\Delta\mu_{\text{fluid, fcc}}$ (dashed line), $\beta\Delta\mu_{\text{fluid, bcc}}$ (dotted line), and $\beta\Delta\mu_{\text{fcc, bcc}}$ (continuous line). Upon increasing P (or ρ), the fluid transforms into a fcc solid; then, a fcc-bcc transition takes place until the bcc melts into a fluid phase again. The lines are spline interpolants of the data points. A zoom on the low-pressure region shows the nonmonotonic behavior of $\beta\Delta\mu_{\text{fcc, bcc}}$, a feature that is ultimately responsible, at higher temperatures, for the reentrance of the bcc phase (see also Fig. 3).

tion of the pressure. Note that, at low pressures, the bcc phase is about to become stable as the fluid freezes into a fcc structure. In fact, this eventually occurs at higher temperatures, in a way not documented before for the GCM.

Upon increasing the temperature, the shallow valley in $\mu_{\text{fcc}} - \mu_{\text{bcc}}$ moves gradually upwards until a narrow range of pressure appears (for $T^* \geq 0.0030$) where a stable bcc phase slips in between the fluid and the fcc solid phases. This is possible because the corresponding increase of the freezing pressure with temperature is not large enough to suppress the reentrant bcc phase. For $T^* > 0.0038$, the fcc phase ceases to be stable and a more regular behavior sets in, similar to that predicted by Lang and co-workers [4].

All in all, the phase diagram represented in Fig. 2 emerges. If compared with Fig. 9 of [4], two differences stand out: a definitely lower triple-point temperature ($T_{\text{tr}}^* \approx 0.0031$) and the as yet unpredicted reentrance of the bcc phase when the fcc solid is isothermally expanded for reduced temperatures in the 0.0031–0.0037 range. In order to check whether this latter feature is a spurious effect due to the finite size of the system, we investigated the bcc-fcc phase coexistence also for larger samples, but we did not register any significant change in the location of the transition points (see the inset of Fig. 2). In the triple-point region, the density jump is ~ 0.002 across the fluid-solid transition and ~ 0.00015 across the solid-solid transition; the corresponding (absolute) values of the entropy jump per particle are $\sim 0.7k_B$ and $\sim 0.1k_B$, respectively. The freezing line attains its maximum value ($T_{\text{max}}^* \approx 0.00874$) for $\rho_{\text{max}}^* \approx 0.239$. At the maximum, the fluid-solid transition is still first-order

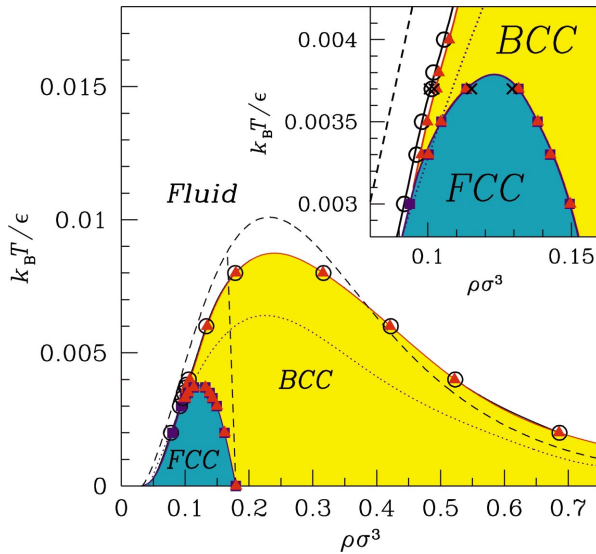


FIG. 2. (Color) Phase diagram of the GCM in the (ρ, T) plane, with a zoom on the triple-point region (inset). The transition densities for each phase are shown for various temperatures: fluid ($N=1372$, black open circles), fcc ($N=1372$, blue solid squares), and bcc ($N=1458$, red solid triangles). The black crosses refer to simulations of larger systems ($N=2048$, fluid and fcc; $N=2000$, bcc) at $T^*=0.0037$. The continuous lines drawn through the data points are a guide for the eye. We also plotted the freezing and the fcc-bcc coexistence loci calculated in [4] (black dashed lines), and the ordering threshold predicted by a one-phase entropy-based criterion (blue dotted line) [12].

with an entropy gap between the two phases equal to $0.79k_B$.

To have a clue on the extent to which statistical errors may affect our conclusions, we turn the reader's attention back to Fig. 1. Let $\Delta\mu_{A,B}(P)$ be the μ gap (at fixed temperature) between two generic phases A and B . In the triple-point region, we estimated a maximum statistical error on the minimum value of $\beta\Delta\mu_{\text{fcc,bcc}}(P)$ approximately equal to 10^{-2} . Of the same order is the maximum error we estimated, near coexistence, on the values of $\beta\Delta\mu_{\text{fluid,solid}}(P)$. However, the rate of change of this latter quantity is much larger, implying that its zero is more sharply defined. This means that fluid-solid coexistence is numerically better defined than solid-solid coexistence. If we follow the evolution of $\beta\Delta\mu_{\text{fcc,bcc}}(P)$ as a function of T (see Fig. 3), we realize that, over the whole stability region of the reentrant bcc phase, this quantity takes values that are of the order of the estimated numerical errors. However, we can safely argue that the true errors are in fact much smaller since, otherwise, we would have hardly obtained the very smooth behavior represented in Fig. 3 as well as the clear phase portrait shown in the inset of Fig. 2. The already mentioned absence of any significant size dependence of $\beta\Delta\mu_{\text{fcc,bcc}}(P)$ at $T^*=0.0037$ is a further guarantee of the reliability of the present phase diagram.

The fcc phase of the GCM is energetically favored at low densities (ρ^* less than ≈ 0.17), for temperatures up to $T^*=0.008$. This may actually explain why the fcc-bcc coexistence locus found in Ref. [4] is an almost vertical line in the ρ - T plane, which leads to a more extended region of fcc

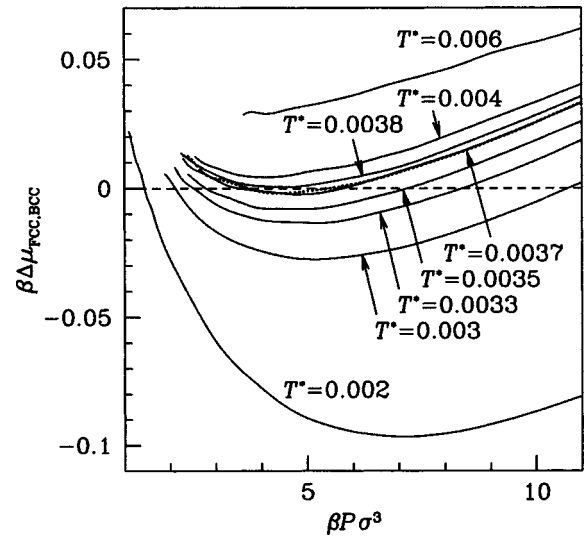


FIG. 3. Temperature evolution of $\beta\Delta\mu_{\text{fcc,bcc}}$, the chemical-potential gap between the fcc ($N=1372$) and bcc ($N=1458$) phases, plotted as a function of the pressure. For $T^*=0.003$ and 0.006 , the systems investigated were smaller (864 and 1024 particles, respectively). The dotted line refers to a calculation carried out at $T^*=0.0037$ using larger samples (fcc: $N=2048$; bcc: $N=2000$), and was plotted for a comparison with the smaller-sizes calculation at the same temperature.

stability. In fact, Lang and co-workers used the Gibbs-Bogoliubov inequality to optimize a strictly harmonic model of both solid phases. This method may actually enhance the crystallinity and give, at the same time, an inadequate representation of the entropic contribution to the solid free energies. Considering that the fcc-bcc transition occurs for rather small densities, the harmonic approximation seems a severe limitation of the theory. In fact, the variational technique basically propagates to higher temperatures the relative stability condition valid at $T=0$. We also note that the fcc-to-bcc transition undergone, with increasing temperatures, by the GCM at low densities is to be ascribed to the higher entropy of the bcc phase, that is likely due to the presence of a larger number of soft shear modes. Even below the triple-point temperature, bcc-ordered grains tend to form in the liquid that is about to freeze, a phenomenon that substantially slows down crystallization.

The low-density and low-temperature phase behavior of the GCM, with a triple point separating a region where the fluid freezes into a fcc structure from another region where these two phases are bridged by an intermediate bcc phase, is rather common among model systems with softly repulsive interactions, such as the inverse-power potential, $v_n(r)=A(\sigma/r)^n$ [13,14], and the Yukawa potential, $v_\ell(r)=B \exp(-r/\ell)/r$ [15–17]. The phase diagram of the above two models is typically unfolded by one or two (possibly rescaled) thermodynamic quantities and by the relevant control parameter of the interaction, i.e., the inverse-power-law exponent $1/n$ or the Yukawa length ℓ . The crystalline pattern produced by such potentials is critically determined by their degree of softness, the bcc phase being promoted by a sufficiently soft interaction. A criterion to relate the phase behav-

ior of $v_n(r)$ and $v_\ell(r)$ to that of the GCM is to require the logarithmic derivatives of such potentials to match that of the Gaussian potential [Eq. (1)], at least for separations close to the mean interparticle distance, $\bar{r} = \rho^{-1/3}$. The values of n and ℓ that enforce this mapping are

$$\tilde{n} = 2\rho^{*-2/3} \text{ and } \tilde{\ell} = \frac{\rho^{*1/3}\sigma}{2 - \rho^{*2/3}}. \quad (2)$$

When ρ^* increases along the GCM freezing line, the bcc phase becomes eventually stable. The same effect occurs with the inverse-power and Yukawa potentials when $1/n$ and ℓ change with the freezing density according to Eq. (2). In this respect, $1/n$ and ℓ play a role analogous to that of an effective temperature. For instance, dilute solutions of charged colloids with counterions [18], which constitute a practical realization of $v_\ell(r)$, show this kind of behavior as a function of the Debye screening length.

The phase diagram of the GCM shows some resemblance also with the phase behavior of star-polymer solutions [8]. At

low densities, the arm number f plays the role of an effective inverse temperature (for two reasons: the strength of the potential increases with f and its range increases with f^{-1}). For not too huge values of f , the Yukawa repulsion yields a phase-stability scenario that is very similar to that of the GCM. Only for star-polymer packing fractions larger than ~ 0.7 (which is where the nearest-neighbor distance in a bcc solid is $\sim \sigma$) will the peculiarities of the short-distance repulsion make a difference, stabilizing other cubic phases that are likely unstable in the GCM.

In this paper, we discussed the phase diagram of the GCM that was redrawn using current best-quality numerical-simulation tools. We predicted the existence of a narrow range of temperatures within which the sequence of stable phases exhibited by the GCM upon isothermal compression is fluid, bcc, fcc, bcc again, and finally fluid again. We also rationalized these findings in terms of the properties of other softly repulsive potentials, with an emphasis on the phase behavior of star-polymer solutions.

We acknowledge some useful discussions with Gianpiero Malescio.

-
- [1] C. N. Likos, M. Watzlawek, and H. Löwen, *Phys. Rev. E* **58**, 3135 (1998).
 [2] M. Schmidt, *J. Phys.: Condens. Matter* **11**, 10163 (1999).
 [3] F. H. Stillinger, *J. Chem. Phys.* **65**, 3968 (1976).
 [4] A. Lang, C. N. Likos, M. Watzlawek, and H. Löwen, *J. Phys.: Condens. Matter* **12**, 5087 (2000).
 [5] C. N. Likos, *Phys. Rep.* **348**, 267 (2001).
 [6] A. A. Louis, P. G. Bolhuis, J. P. Hansen, and E. J. Meijer, *Phys. Rev. Lett.* **85**, 2522 (2000); P. G. Bolhuis, A. A. Louis, J. P. Hansen, and E. J. Meijer, *J. Chem. Phys.* **114**, 4296 (2001).
 [7] F. H. Stillinger, *Phys. Rev. B* **20**, 299 (1979).
 [8] M. Watzlawek, C. N. Likos, and H. Löwen, *Phys. Rev. Lett.* **82**, 5289 (1999).
 [9] B. Widom, *J. Chem. Phys.* **39**, 2808 (1963).
 [10] D. Frenkel and A. J. C. Ladd, *J. Chem. Phys.* **81**, 3188 (1984).
 [11] J. M. Polson, E. Trizac, S. Pronk, and D. Frenkel, *J. Chem. Phys.* **112**, 5339 (2000).
 [12] P. V. Giaquinta and F. Saija, *Chem. Phys. Chem.* (to be published).
 [13] B. B. Laird and A. D. J. Haymet, *Mol. Phys.* **75**, 71 (1992).
 [14] R. Agrawal and D. A. Kofke, *Phys. Rev. Lett.* **74**, 122 (1995).
 [15] M. O. Robbins, K. Kremer, and G. S. Grest, *J. Chem. Phys.* **88**, 3286 (1988).
 [16] E. J. Meijer and D. Frenkel, *J. Chem. Phys.* **94**, 2269 (1991).
 [17] S. Hamaguchi, R. T. Farouki, and D. H. E. Dubin, *Phys. Rev. E* **56**, 4671 (1997).
 [18] E. B. Sirota, H. D. Ou-Yang, S. K. Sinha, and P. M. Chaikin, *Phys. Rev. Lett.* **62**, 1524 (1989).